Article

Evaluation of Cobalt, Nickel, and Palladium Complexes as Catalysts for the Hydrogenation and Improvement of Oxidative Stability of Biodiesel

Fortunate P. Sejie [1,2,*], Olayinka A. Oyetunji [1], Banothile C. E. Makhubela [3], James Darkwa [3,4] and Nora H. de Leeuw [2,5,*]

[1] Department of Chemistry, University of Botswana, Gaborone Private Bag UB 00704, Botswana; yoyetunji@gmail.com
[2] School of Chemistry, Cardiff University, Cardiff CF10 3AT, UK
[3] Department of Chemical Sciences, University of Johannesburg, P.O. Box 524, Auckland Park 2006, South Africa; bmakhubela@uj.ac.za (B.C.E.M.); jdarkwa@gmail.com (J.D.)
[4] Botswana Institute for Technology Research and Innovation, Gaborone Private Bag 0082, Botswana
[5] School of Chemistry, University of Leeds, Leeds LS2 9JT, UK
* Correspondence: sejiep@ub.ac.bw (F.P.S.); n.h.deleeuw@leeds.ac.uk (N.H.d.L.)

Abstract: Developing effective catalysts that can selectively hydrogenate C=C bonds in biodiesel samples is vital as it tackles the major problem of oxidative stability, which greatly limits the utilization of biodiesel as an alternative fuel. In this work, Co, Ni, and Pd catalysts stabilized with the bidentate nitrogen ligands N-(3-(triethoxysilyl)propyl)pyridin-2-ylmethylimine and N-(3-(triethoxysilyl)propyl)picolinamide were synthesized, characterized, and used as pre-catalysts in the transfer hydrogenation of C=C bonds in fatty acid methyl esters. The active catalysts from the Co, Ni, and Pd complexes sequentially hydrogenate the C18:2 chains to C18:1, which is further converted to C18:0 in the FAMEs of both methyl linoleate and jatropha biodiesel. The hydrogenation process was kinetically controlled, and after 3 h it yielded a biodiesel sample that contained 25.83% C16:0, 12.52% C18:2, 41.54% C18:1, 14.47% C18:0 and 3.0% C18:2 isomers. The un-hydrogenated jatropha diesel, hydrogenated jatropha diesel, and a B20 blend of jatropha were tested for susceptibility to oxidation reactions using the Rancimat method and FTIR spectroscopy, and the partial hydrogenation had improved the induction period by 3 h.

Keywords: biodiesel hydrogenation; oxidative stability; Rancimat method; homogeneous catalysis

1. Introduction

Biodiesel is the most valuable natural fuel, which is composed of multi-unsaturated and saturated substrates [1]. Converting inedible vegetable oil to biodiesel is a popular approach to generating renewable fuel. However, the high degree of poly-unsaturation in biodiesel leads to auto-oxidation reactions during storage. These oxidation reactions are initiated by light or high temperatures [2], and the radical auto-oxidation reactions lead to the formation of peroxides, fatty acid radicals, alcohols, and water, which cause poor fuel performance in vehicles [3,4]. The high degree of poly-unsaturation lowers fuel stability and causes low ignition [5] and it is also reported to affect the cold flow properties of diesel. However, when both the degrees of saturation and unsaturation are optimized through partial hydrogenation, excellent fuel properties can be achieved. To solve the problem of the low oxidative stability of biodiesel, adding antioxidants, blending with commercial diesel, and partial hydrogenation are often employed [6–8]. However, these other methods are expensive compared to partial hydrogenation of the fatty acid methyl esters (FAME) using heterogeneous or homogeneous catalysts, which can discriminate between the closely related moieties that are present in the FAMEs [8].

The use of hydrogen donors instead of hydrogen gas allows much slower reaction kinetics, which can influence the partial hydrogenation of the C-C double bonds present in the long-chain substrates [9]. It has been established from recent literature reports, that partial hydrogenation of unsaturated FAMEs can improve low oxidative stability by converting poly-unsaturated components to mono-unsaturated components, which are then further converted to fully saturated components [10]. However, the production of biodegradable wax (saturated components of the biodiesel), as well as cis- and trans-isomerism, are always difficult to avoid during hydrogenation reactions using either homogeneous or heterogeneous catalysts. It has been shown in the literature that the partial hydrogenation of biodiesel using homogeneous catalysts/metal complexes improves the oxidative stability of biodiesel concerning the induction period (IP) [11–13]. For example, Kongprawes and co-workers have reported an improved oxidative stability of plasma-hydrogenated biodiesel from 2.13 to 5.45–10 h, whereas another study on soybean biodiesel hydrogenation using Pd, Ni, and Pt catalysts supported on SiO_2 has shown that the induction period of the biodiesel increased from 2 to 10.4, 4.8, and 2.7 h, respectively, for the Pd-, Pt-, and Ni-catalyzed reactions over a 4 h reaction time [14,15].

Hydrogen donors are also used to reduce the C=C content in biodiesel, leading to an improved IP, as demonstrated, for example, in a study using glycerol as a hydrogen donor to hydrogenate palm oil, where the IP was reported to increase from 17.7 to 23 h [16]. Oxidative stability measured by the Rancimat method is one method that has been used to detect the number of water-soluble volatiles that are released by the biodiesel. When the biodiesel is heated, released volatiles are passed through distilled water, and the time taken for the electrical conductivity of the water to change is reported as the induction period (IP) [17–19]. This method was used together with infrared spectroscopy to study the changes in the functional groups of the biodiesel [20].

This work aligns with the UNEP-UN environmental program, goal number 12, which targets reducing fossil fuel subsidies as a way of reducing carbon emissions and promoting a green economy. We report the synthesis and characterization of the Pd-, Ni-, and Co-based catalysts and their application as promoters in the transfer hydrogenation of methyl linoleate and biodiesel samples. These hydrogenation reactions attempt to lower the oxidative stability of the biodiesel samples without an overall change in the fuel properties. The changes in the oxidative stability of the hydrogenated biodiesel samples in comparison to the commercial diesel LP5 and a blend of the biodiesel with LP5 are also investigated.

2. Results and Discussion

2.1. Synthesis and Characterization of the Ligand **L2** and Their Cobalt, Nickel, and Palladium Complexes (**C4**, **C5**, and **C6**)

In this work, the bidentate ligands N-(3-(triethoxysilyl)propyl)pyridin-2-ylmethylimine (**L1**) and N-(3-(triethoxysilyl)propyl)picolinamide (**L2**) were used as suitable stabilizers for the divalent Pd, Ni, and Co metal complexes. **L1** can coordinate to the metal centers through the two nitrogen atoms, while in **L2**, the nitrogen atom is electron-deficient compared to the one in the imine ligand, which causes ligand **L2** to bind less strongly through the donor nitrogen atoms compared to the electron-rich imine ligand. However, the presence of the electron-rich silicon atom in both ligands often leads to reduced effects of electron deficiency on the donor atoms. The cobalt (**C1-Co**), nickel (**C2-Ni**), and palladium (**C3-Pd**) complexes of ligand **L1** were synthesized according to methods reported in the literature [21,22]. The scheme for the synthesis of ligand **L1** and the metal complexes **C1-Co**, **C2-Ni**, and **C3-Pd** is shown in Scheme 1a. Ligand **L2** was obtained as a highly viscous brown oil, and its characterization is detailed in the electronic supporting information (ESI), with the results captioned as Figures S1–S4. To synthesize the corresponding amide complexes, **L2**; N-(3-(triethoxysilyl)propyl)picolinamide was dissolved in a minimum amount of dichloromethane and 0.001 mol NaOH in methanol [23,24]. The metal precursors ($CoCl_2$, $NiBr_2(DME)$, or $PdCl_2(NCME)_2$) were suspended in dichloromethane and added to a solution of ligand (**L2**) and stirred at room temperature for 24 h to produce complexes

C4-Co, **C5-Ni**, or **C6-Pd**, respectively (Scheme 1b). The complexes were isolated over a minimum amount of diethyl ether (**C4-Co**) and hexane (**C5-Ni**, **C6-Pd**).
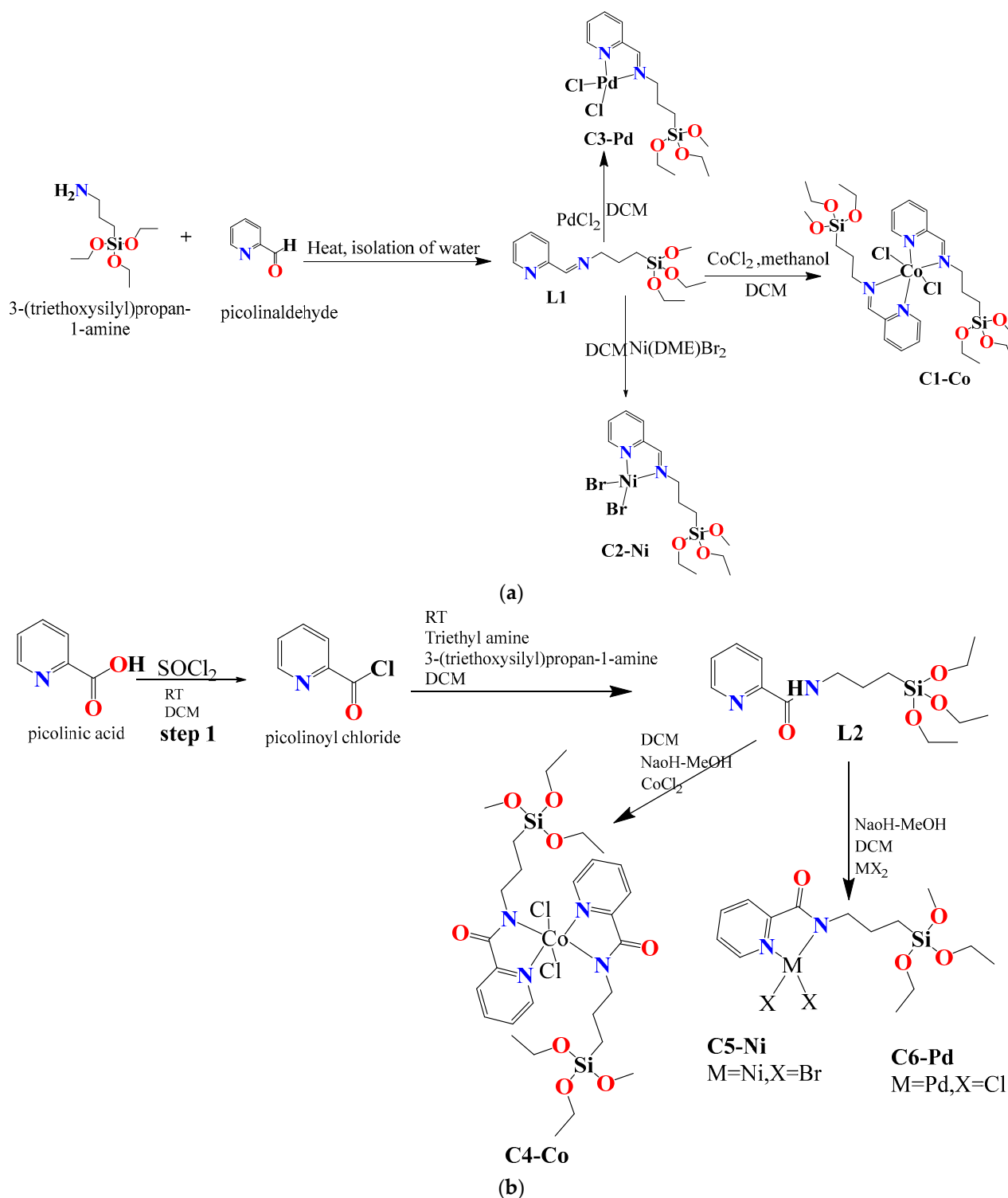
Scheme 1. (**a**) Reaction scheme for the synthesis of ligand **L1** and the corresponding metal complexes. (**b**) Reaction scheme for the synthesis of ligand **L2** and the corresponding metal complexes.

^{1}H NMR and ^{13}C{^{1}H} NMR were used to study the structure of complex **C6-Pd**. The ^{13}C{^{1}H} NMR spectrum is shown in Figure S5. The ^{1}H NMR spectrum in Figure S1 was compared to the one in Figure 1. The coordination of the ligand to the Pd metal center is

confirmed by the absence of the proton on the donor amide nitrogen (proton e, in Figure 1). In addition, the protons adjacent to the donor amide nitrogen shifted from 2.89 ppm (labeled f in Figure S1) to 3.89 ppm (labeled e in Figure 1). This up-field shift in the chemical shift is caused by the de-shielding effects that arise from the donation of the electron from the amido nitrogen to the metal center; these protons were observed up-field to the ethoxy protons, but they appear downfield of the ethoxy protons after coordination of the ligand to the metal center. The aromatic pyridine proton shifts from 8.23 ppm to 8.46 ppm, which also confirms the coordination of the ligand to the metal center.
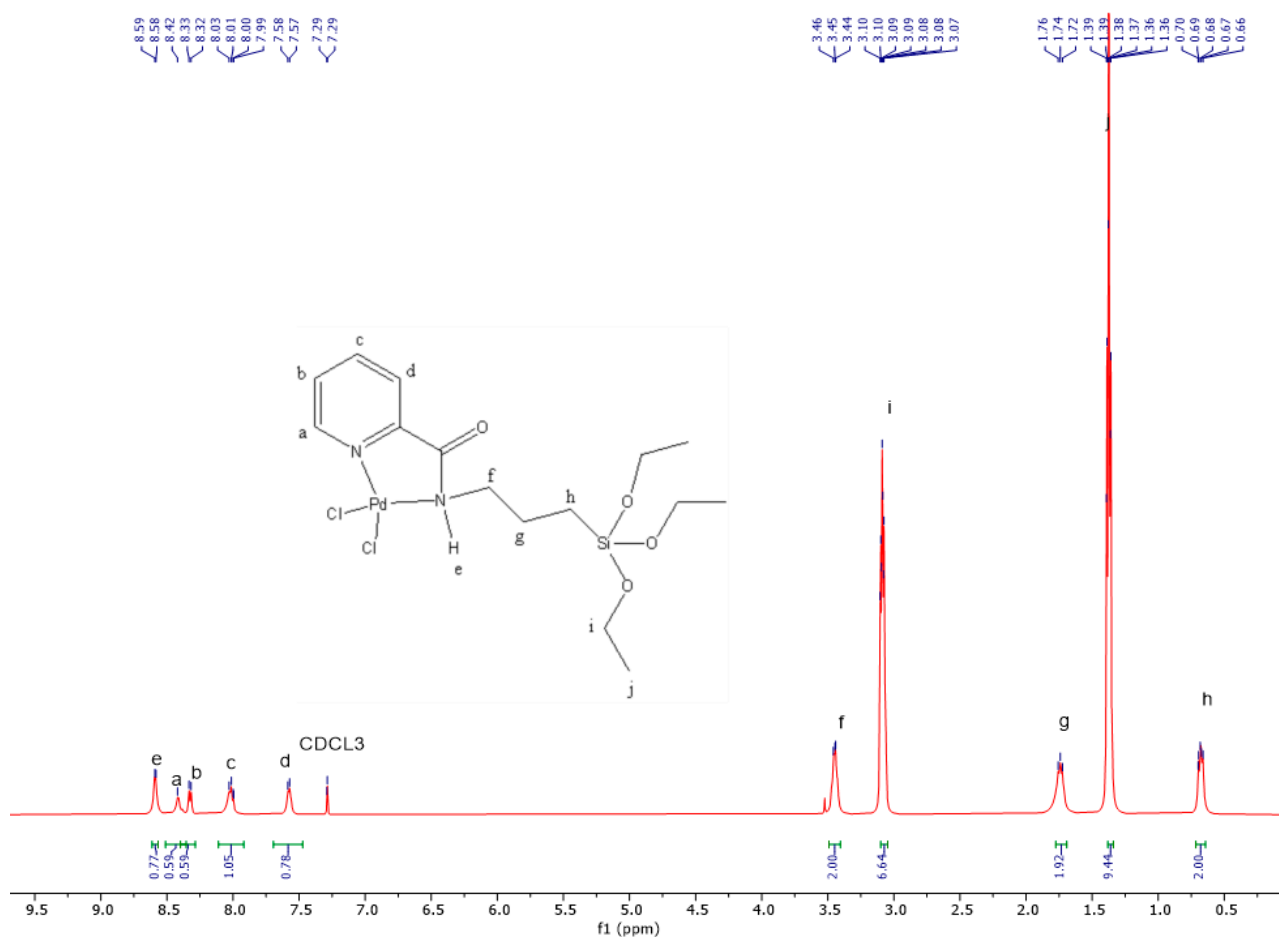

Figure 1. The structural determination of complex **C6-Pd** using ^{1}H NMR.

From the IR spectra in Figure S6a–c, the absence of the N-H stretch peak confirms the formation of the metal complexes. The peak in the region (3300–3400) cm^{-1} is attributed to the C-H stretching frequency. The C=O stretch is observed as a sharp intense peak in the range of 1620 to 1720 cm^{-1} for all three complexes. The aromatic imine stretch is observed in the region of 1560–1580 cm^{-1}. The vibrational modes of the complexes **C4-Co**, **C5-Ni**, and **C6-Pd** further confirmed complex formation. The mass fragmentation of the catalysts was studied using a mass spectrometer with an electrospray ionizer. The detected mass fragments for the complexes are shown in Table 1 alongside the elemental analysis results (the found and expected values). The ESI-MS of the three metal complexes is shown in Figure S7a–c. The mass fragments confirm the formation of the complexes, and the elemental analysis results further provide substantial evidence for the formation of the complexes as expected.

Table 1. The tabulated ESI-MS fragments of complexes **C4-Co**, **C5-Ni**, and **C6-Pd**.

| Complex	Fragment *m/z*	Identification of Fragment	Elemental Analysis Found (Expected)
C4-Co	816.3	$[CoL_2X_2 + K]^+$	C:39.79 (39.48) H:7.97 (8.7) N:6.55 (6.1)
	547.28	$[CoLX + S + K]^+$	
C5-Ni	540.15	$[NiLX_2 + H]^+$	C:34.91 (33.6) H:4.67 (4.81) N:5.55 (5.14)
	180.10	$[NiLX_2 + 3H]^{+3}$	
	286.41	$[NiLX_2 + H + K]^{+2}$	
C6-Pd	505.3	$[PdLX_2 + H]^+$	C:33.95 (35.8) H:6.78 (5.2) N:6.23 (5.6)
	302.99	$[PdLX_2 + S + Na + H]^{+2}$	

L is ligand, X is Cl/Br (Halide), S is solvent—DCM.

2.2. Hydrogenation of Methyl Linoleate and Jatropha Biodiesel

We investigated the transfer hydrogenation of the FAMEs using formic acid as a hydrogen donor. This study aims to establish the catalytic activity of the catalysts and to establish the reaction conditions under which fully saturated products are detected.

2.2.1. Preparation of Fatty Acid Methyl Esters from Fatty Acids

To produce biodiesel from the crude seed oils, fatty acid methyl esters of both jatropha diesel and used sunflower oil were produced through transesterification of the crude oils using potassium hydroxide (KOH) and methanol [21]. In a typical reaction, 100 g of biodiesel was reacted with 40 mL of methanol and 1 g of KOH. The reaction was carried out at 60 °C for 6 h (Scheme 2). The reaction mixture was then cooled, and glycerol was removed using a separating funnel. The biodiesel was washed with three portions of cold distilled water (20 mL) and then dried at 110 °C. The ^{1}H NMR spectra of methyl linoleate and jatropha biodiesel are shown in Figures S8 and S9, respectively. In Figure S8, the disappearance of peak j at 11.15 ppm confirms the absence of the acid hydroxy moiety, while a new peak g in the top spectrum confirms the presence of the methoxy protons at 3.63 ppm, confirming a successful transesterification process. In Figure S9, the methoxy protons are observed at 3.55, 3.56, and 3.57 ppm for the C16:0, C18:0, C18:1, and C18:2 components in the synthesized jatropha biodiesel.
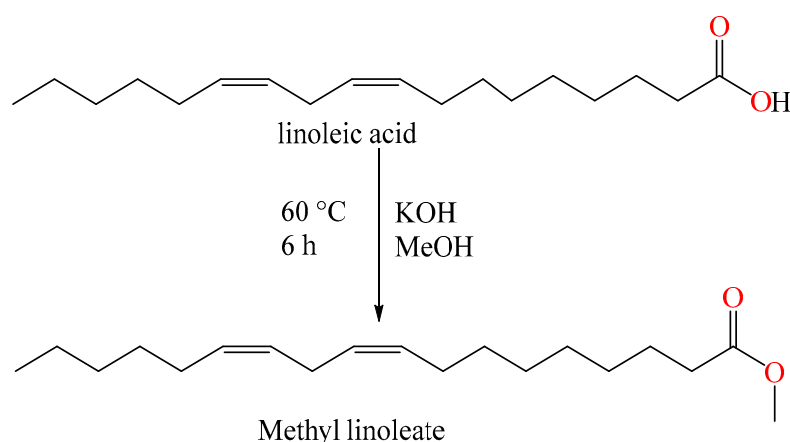
Scheme 2. Transesterification of linoleic acid.

2.2.2. Hydrogenation of Methyl Linoleate

To test the catalytic performance of the prepared metal complexes, methyl linoleate (ML) was used as a source of pure C18:2 components. The best conditions for the catalysis study (catalyst loading and temperature) were those established for **C1** and **C2** in a previous study [22]. Table 2 shows the catalytic activity in the hydrogenation of methyl linoleate using catalysts **C1-Co** to **C6-Pd**. Table 2 entries 1–3 show the catalytic performance of catalysts **C1-Co**, **C2-Ni**, and **C3-Pd** in the transfer hydrogenation of methyl linoleate. The observed compositions of the samples after hydrogenation are [C18:0, 86%; C18:1, 14%; C18:2, 0%], [C18:0, 96%; C18:1, 4%; C18:2, 0%], and [C18:0, 100%; C18:1, 0%; C18:2, 0%] for the **C1-Co**, **C2-Ni**, and **C3-Pd** catalysts, respectively. From entries 3 to 6, it is evident that catalysts **C4-Co**, **C5-Ni**, and **C6-Pd** are efficient as they convert 100% of the C18:2 to C18:0 without any waste side products. From the two sets of catalysts used (imine complexes [**C1-C3**] and amide complexes [**C4-C6**]), the imine complexes **C1-Co** and **C2-Ni** exhibited lower percentages of C18:0 compared to their amide analogs **C4-Co** and **C5-Ni** (entries 1, 2, 4, and 5). The amide-containing catalysts **C4-Co** and **C5-Ni** have higher catalytic activities compared to their imine analogs (**C1-Co** and **C2-Ni**). The Pd catalysts (**C3-Pd** and **C6-Pd**) show even higher catalytic activities compared to the Ni and Co counterparts (**C1-Co**, **C2-Ni**, and **C4-Co**, **C5-Ni**). The higher catalytic activities of the amide-containing catalysts can be attributed to the electron-withdrawing ability of the bridging C=O unit in the ligand, which makes the metal center in the amide-containing catalysts more electrophilic compared to the imine-containing catalysts. When the reaction time was reduced from 12 h to 6 h (entry 7), to determine the extent to which the active catalysts will produce 100% of the saturated product, the product obtained contains 3.21% of C18:0, whereas the detected quantities of C18:1 and C18:2 are 28.47% and 68.20%, respectively. This observation shows that a shorter time allows for partial hydrogenation of the biodiesel that can be used to control the composition of the products formed. Figure S10 shows the changes in the flow of the oil after hydrogenation of all the C=C bonds to form a biodegradable wax.
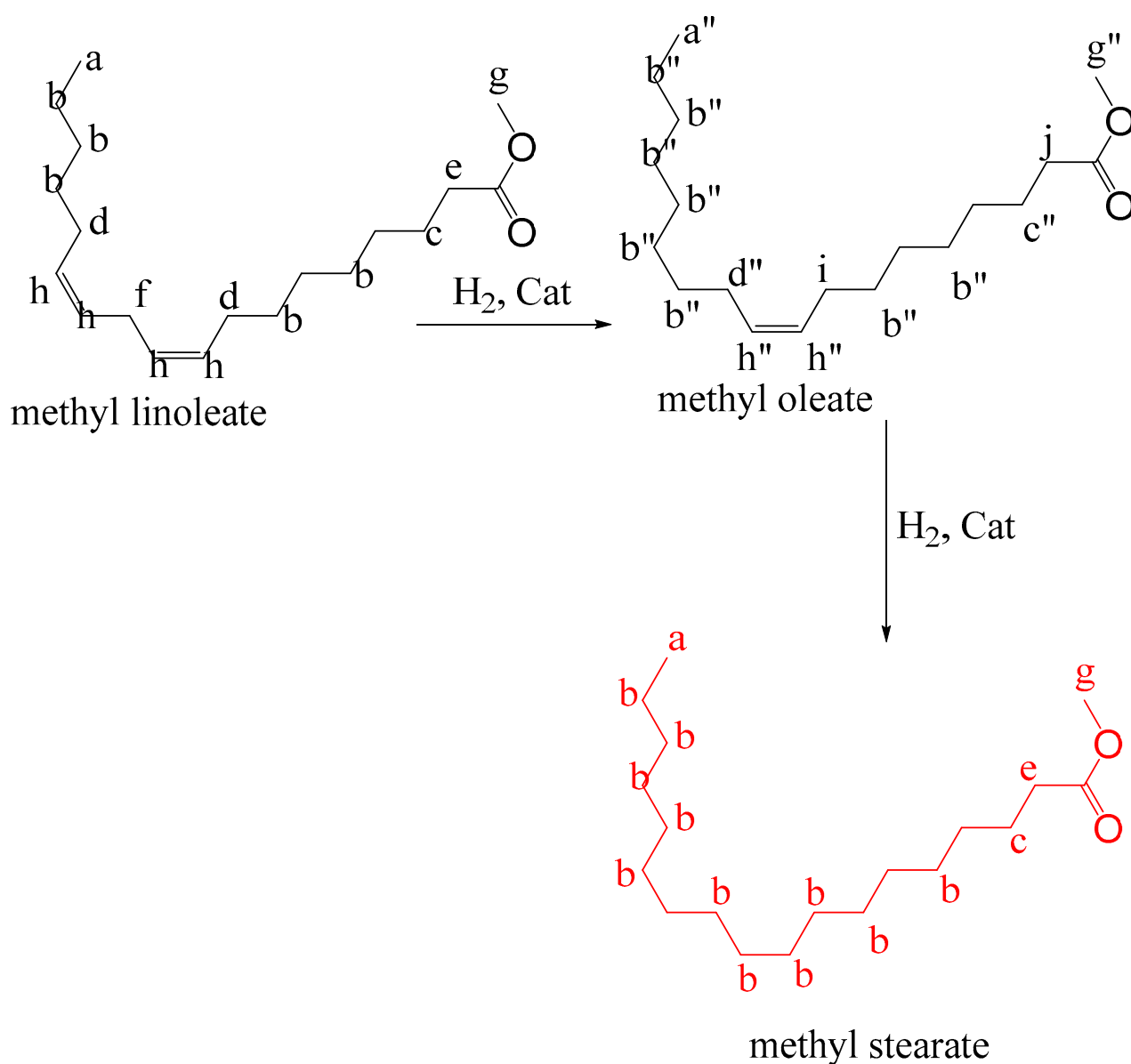
Table 2. Transfer hydrogenation of methyl linoleate.

Entry	Catalyst	Substrate	Composition of Mixture (%)		
			C18:0	**C18:1**	**C18:2**
1	**C1-Co**	ML	86	14	0
2	**C2-Ni**	ML	96	4	0
3	**C3-Pd**	ML	100	0	0
4	**C4-Co**	ML	100	0	0
5	**C5-Ni**	ML	100	0	0
6	**C6-Pd**	ML	100	0	0
7*	**C6-Pd**	ML	3.21	28.47	68.20

Reaction conditions: (ML 0.44 g, catalyst: 0.1 mol%), 12 h, 120 °C, Formic acid (40 mmol), KOH (10 mmol), (ML = Methyl linoleate), 7* time = 6 h. Reaction mixture components were analyzed using GC-MS and ^{1}H NMR.

NMR Kinetic Studies

Scheme 3 shows possible intermediates formed when the C=C in methyl linoleate is hydrogenated. ML (C18:2) is reduced to form methyl stearate (C18:0) through the formation of methyl oleate (C18:1) that is converted to component C18:0, which is undesirable if produced in high amounts. A ^{1}H NMR kinetic study was carried out to determine the extent to which the C18:2 components are reduced with respect to time.

Scheme 3. Hydrogenation of methyl linoleate to methyl stearate through the formation of methyl oleate as an intermediate. Letters a–h represent the protons expected from the labelled components of fatty acid methyl esters.

The ^{1}H NMR spectra of the reaction mixtures following hydrogenation of methyl linoleate using catalyst **C6-Pd** are shown in Figure 2. This sample was analyzed before the reaction was started, at time 0, and further sampling was done after 6 and 12 h. It is evident that the catalyst sequentially converts C18:2 to C18:1 and finally to C18:0. The results show that product selectivity is dependent on the kinetic control of the reaction, and the partial hydrogenation reaction conditions can be achieved by optimizing the catalysis time.
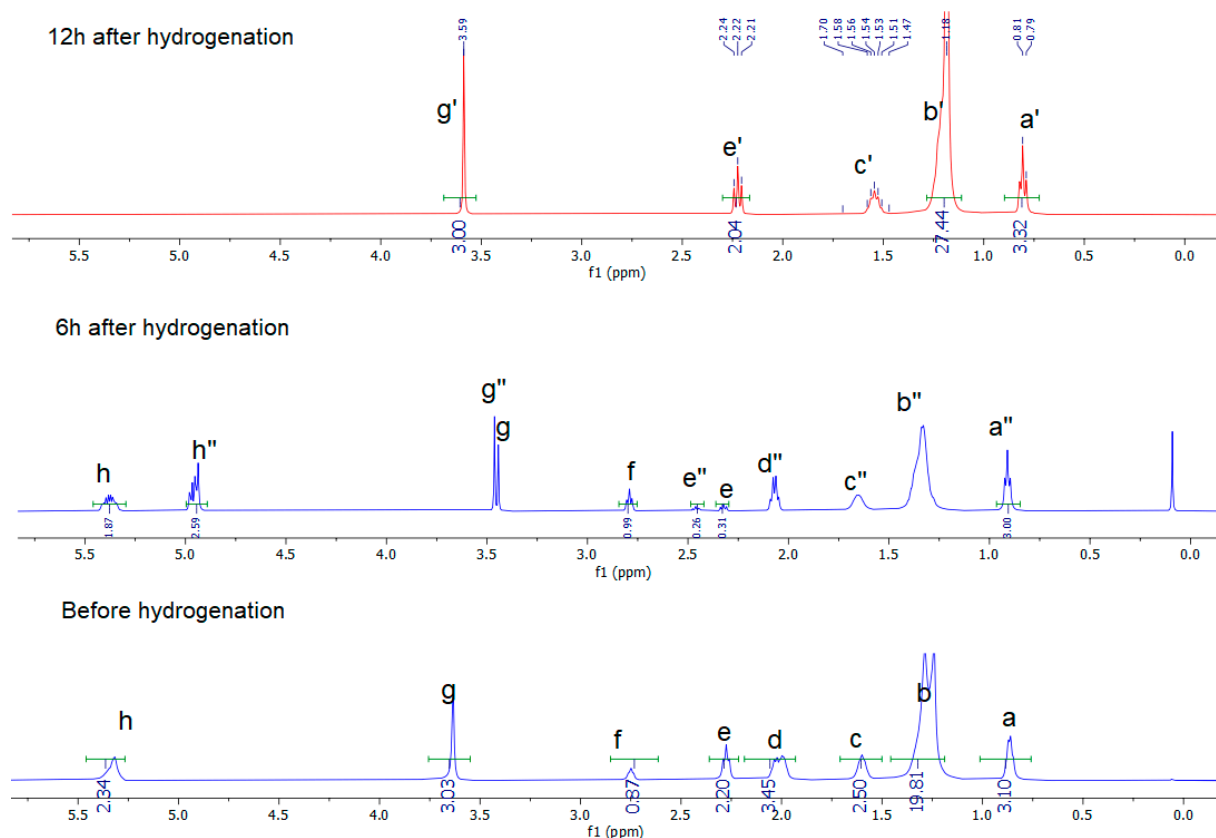
Figure 2. ^{1}H NMR spectra of the reaction mixture in the hydrogenation of methyl linoleate using catalyst **C6-Pd** sampled at different reaction times. Reaction conditions: ML (0.44 g), formic acid (40 mmol), catalyst (2.3×10^{-5} mol), KOH (10 mmol), 120 °C, DCM solvent. Letters a–h represent the corresponding chemical shifts of the protons labelled in Scheme 3.

2.2.3. Transfer Hydrogenation of Jatropha Biodiesel

To investigate the efficiency of the catalysts in converting multiple long-chain components of biodiesel in a sample, jatropha biodiesel was used as a substrate. From the study, only one component (C18:2) was present in the mixture. Figure 3 shows an example of the gas chromatogram of the Tonota jatropha biodiesel (BD1) before hydrogenation. The chromatogram shows the peaks corresponding to the C18:2 and C18:1 components in the biodiesel (at retention times of 17.39 and 17.34 min, respectively), C18:0 at 17.69 min, and the C16:0 peak at 15.7 min. The corresponding mass fragments and percentages of the components are shown in Figure S11 and Table S1, respectively).
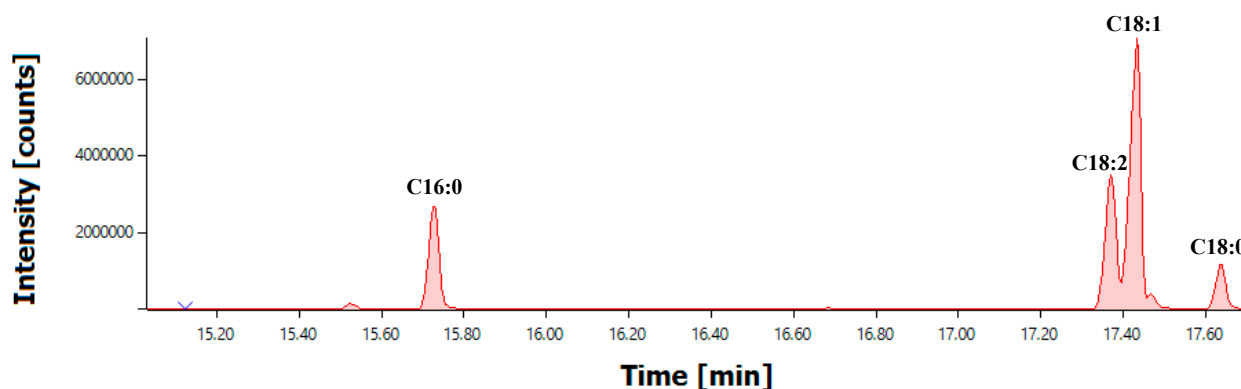

Figure 3. Gas chromatogram of Tonota jatropha biodiesel (BD1) before hydrogenation.

Figure 4 shows an example of the gas chromatogram of hydrogenated Tonota jatropha biodiesel (BD1). The figure shows the observed changes in the chromatogram after the hydrogenation of BD1, with an increase in the intensity of the peak at a retention time of 17.74 min, which corresponds to the presence of the C18:0 component, with m/z of 298. Figure S12 indicates that these components have been hydrogenated to yield the C18:0 component for entry 2. In both Figure 3 (BD1 before hydrogenation) and Figure 4 (jatropha biodiesel after hydrogenation), a peak at a retention time of 15.72 min, which has been attributed to the presence of the C16:0 component, shows no change after hydrogenation.
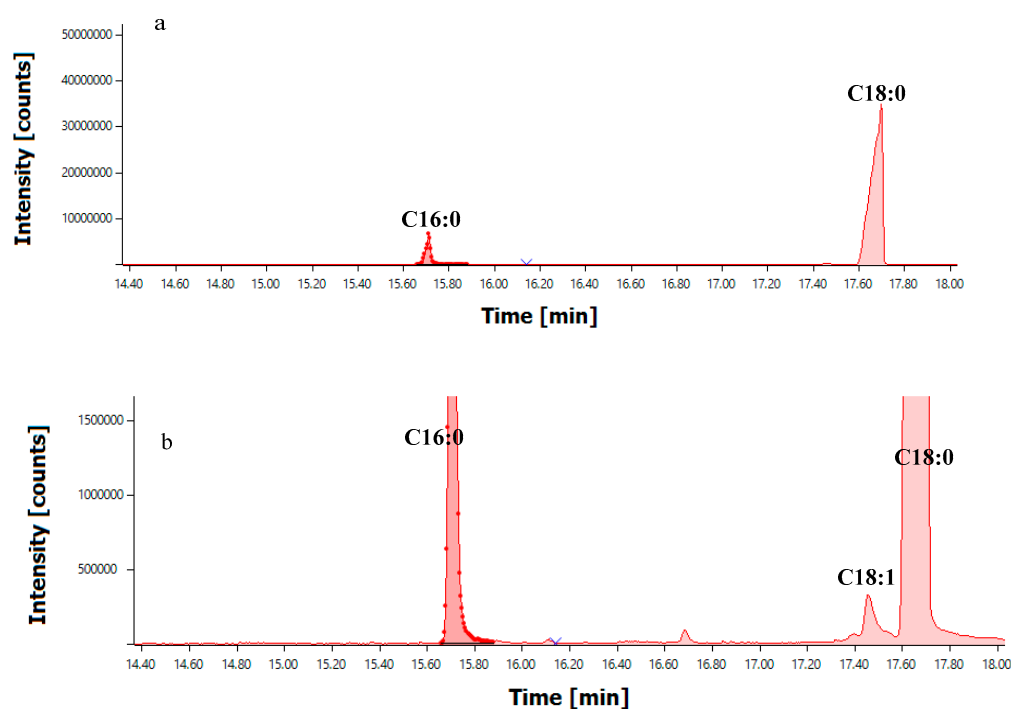

Figure 4. An example of the gas chromatogram of the reaction mixture after 12 h of hydrogenation of BD1 using **C4** (**a**) with a zoomed-in area of the chromatogram (**b**) showing the C18:1 component.

Table 3 shows the product composition of BD1 after hydrogenation using catalysts **C1-Co**, **C2-Ni**, **C3-Pd**, **C4-Co**, **C5-Ni**, and **C6-Pd**. The hydrogenation reactions were carried out under reaction conditions established for the hydrogenation of methyl linoleate. The temperature was increased to 140 °C for a reaction time of 3 h for improved hydrogenation of several unsaturated components in the biodiesel samples. Entries 1–3 show the catalytic performances of catalysts **C1-Co**, **C2-Ni**, and **C3-Pd**, with the three catalysts having converted all the C18:1 and C18:2 to C18:0 components, which correlates well with the observations in Table 2. Entries 4–6 show that <90% of C18:1 and C18:2 in BD1 is converted to the C18:0 component using catalysts **C4-Co**, **C5-Ni**, and **C6-Pd**. In this study (Table 3 entry 7[a]), reducing the reaction time to 3 h improves the percentage of C18:1 in the mixture. From entry 7, the amount of C16:0 is expected to remain constant at approximately 13%, as the component does not contain any C=C that can be further converted to a product. The C16:0 and C18:0 components do not undergo oxidation reactions as they do not have C=C bonds and they do not contribute directly to the oxidative stability of a biodiesel sample, although they do affect the viscosity of the samples. The oil sample isolated at this entry (hereafter referred to as H-BD1) has the following composition: 23.4%, 8.1%, 49.2%, and 18.2% of C16:0, C18:2, C18:1, and C18:0, respectively. After hydrogenation, new peaks of compounds with m/z of 294 (2.1%) were observed at retention times between 19.1 and 19.5 min (Figure 5), which are suggested to be isomers of the C18:2 chain, as they were not observed before hydrogenating the sample. The mass fragments for the observed compounds are shown in Figure S13. The trans-isomerism of the C=C bonds in fatty acid

methyl esters during hydrogenation has also been reported to be common in the Pd- and Ni-catalyzed reactions [7].

Table 3. Hydrogenation of jatropha curcas biodiesel.

Entry	Catalyst	Composition of Product (%)				
		C16:0	C18:2	C18:2 Isomers	C18:1	C18:0
	Initial composition BD1	13.45	18.1	-	64.11	4.00
1	**C1-Co**	13.1	0	-	0	86.8
2	**C2-Ni**	13.2	0	-	0	86.7
3	**C3-Pd**	13.3	0	-	0	86.3
4	**C4-Co**	13.2	0	-	1.89	85.0
5	**C5-Ni**	13.1	0	-	3.14	83.7
6	**C6-Pd**	13.3	0	-	5.64	81.2
7[a]	**C6-Pd**	25.83 [#]	12.5	3.01	41.54	14.48

Reaction conditions: Substrate (1.0 g), formic acid (40 mmol), catalyst (0.1 mol%), KOH (10 mmol), 140 °C, reaction time 6 h, DCM solvent, 7[a] reaction time 3 h. [#] It is rather odd that the composition of C16:0 appears to have increased for a component of the product that is saturated, which is likely due to an unknown impurity that may have been in the sample analyzed. All other peak compositions at a reaction time of 3 h are accurate.
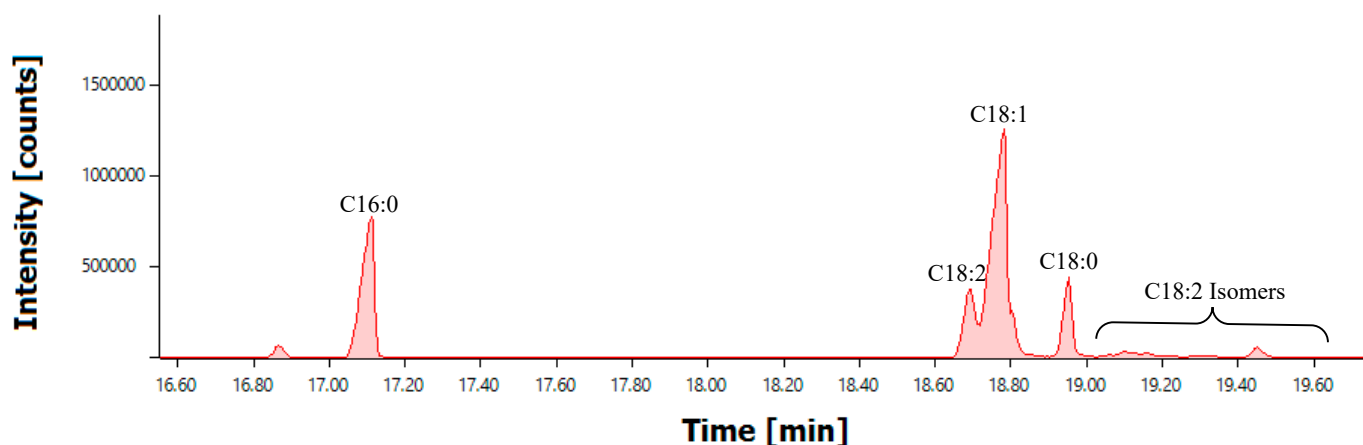

Figure 5. An example of the GC chromatogram of the reaction mixture obtained for entry 7[a] in Table 3.

Catalyst **C6-Pd** was used to hydrogenate other biodiesel samples over a 3 h reaction time to achieve partially hydrogenated biodiesel samples that can be further tested for oxidation reactions. Table 4 shows the changes in the long chain components after hydrogenation of BD2 and BD3 using catalyst **C6-Pd** at a 3 h reaction time. From this study, the accumulation of C18:2 isomers is observed to be less than 10% after a 3 h reaction time. The diesel composition after hydrogenation shows a decrease in C18:2 and an increase in C18:1, while C18:0 increases by a small percentage (Figures S14 and S15). The catalysts used in this study were previously applied to hydrogenate short-chain substrates. Mercury poisoning tests were conducted to determine whether the catalysis process was heterogeneous or homogeneous. For the **C6-Pd** catalyst, the mercury poisoning tests on various substrates showed a 50% decline in catalytic activity, attributed to the formation of Pd black after the catalysis cycle, as confirmed by transmission electron microscopy [23]. In contrast, no metal nanoparticles were observed after reactions with the **C4-Co** and **C5-Ni**, and the mercury poisoning tests showed only a minimal decline in catalytic activity. For the **C1-Co-**, **C2-Ni-**, and **C3-Pd**-catalyzed reactions, no metal nanoparticles were detected, and the mercury

poisoning tests showed less than a 50% decrease in catalytic activity [22]. Therefore, the **C6-Pd** catalyst promotes a heterogeneous process, as it dissociates to form metallic species responsible for the observed catalytic activity. In contrast, the **C1-Co**, **C2-Ni**, **C3-Pd**, **C4-Co**, and **C5-Ni** catalysts function as homogeneous catalysts and do not dissociate to form metallic species.

Table 4. Hydrogenation of Maun jatropha and used sunflower biodiesel.

	Maun Jatropha (BD3)		Used Sunflower Oil (BD2)	
	Product Composition (%)		Product Composition (%)	
	Before	After	Before	After
C16:2	0.089	0	0	0
C16:0	18.79	20.2	9.7	18.23
C18:2	40.8	25.75	71.9	25.9
C18:1	34.4	30.44	14.1	45.3
C18:0	5	16.23	2.9	7.5
C18:2 isomers	0	7.38	0	3.07

Reaction conditions: Substrate (1.0 g), formic acid (40 mmol), catalyst **C6-Pd** (0.1 mol%), KOH (10 mmol), 140 °C, DCM solvent, reaction time 3 h.

Our observations are in line with literature reports on the hydrogenation of long-chain substrates using a homogeneous Pt (PPh_3)-$(SnCl_2)$ catalyst, where all the C18:2 is converted to C18:1 before further hydrogenation to a C18:0 chain (Table 5 entries 1–7). From the literature, nickel catalysts are reported to yield methyl iso-linoleate as a by-product, but this product was not observed in our study. Further literature findings report similar observations on palladium on carbon (Pd/C) catalysts under mild conditions of 1 atm hydrogen pressure and 75 °C for 2 h [24]. In our study, based on the observed compositions after catalysis using catalysts **C1-Co**, **C2-Ni**, **C3-Pd**, **C4-Co**, **C5-Ni**, and **C6-Pd** in the hydrogenation of both methyl linoleate and BD1, both C18:2 and C18:1 are converted to C18:0 chains, unless the time is reduced. The observed high yield of C18:0 from the hydrogenation of C18:2 and C18:1 is reported to be influenced by the nature of the complex formed between the substrate and the active metal center of the catalysts, as proposed in Figure 6. If the diene (I) interactions are stronger/favored compared to the monoene (II) interactions, then the catalyst will just convert the C18:3 and C18:2 components to C18:1, whereas only negligible amounts of C18:0 will be observed. This proposal has been reported for the hydrogenation of sunflower oil and methyl linoleate using the Pd^0-PEG catalysts, in which just less than 3% of C18:0 is found, with 97% C18:1 [25].
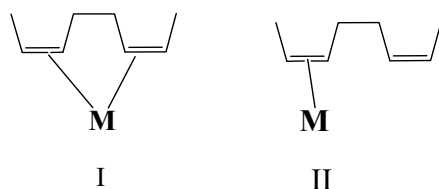

Figure 6. Nature of the complex formed between the substrate and the active metal center of the catalysts, which can take place between the two C=C (I) to through only one C=C (II) interactions.

Table 5. Comparison of the catalysts reported in the literature and those from this study (the selectivity of different catalysts in the hydrogenation of methyl linoleate and biodiesel).

Entry	Catalyst	FAME	Selectivity (%)		Conversion (%)	Time (h)	T (°C)	Reference
			C18:0	C18:1				
1	Fe(CO)$_5$	ML	0	3.4	100	7	150	[26]
2	Fe(CO)$_5$-ML	ML	5.1	33.5	100	7	150	[26]
3	NiCl$_2$DMF	ML	15	85	98.3	24	-	[27]
4	Py$_3$RhCl$_2$DMF	ML	3	95	92.8	24	-	[27]
5	Pd^{0}PEG400	ML	7	93	100	3.2	75	[25]
6	Pd^{0}PEG400	Sunflower	5.4	86.9	98.6	3.2	120	[25]
7	Pt(PPH3)$_2$ClSn	Soybean	0	78.2	95.6	3	90	[28]
8	Pd(C$_3$H$_2$N$_2$Me$_2$)$_2$Cl$_2$	ML	100	-	100	0.5	50	[10]

Entry	Catalyst	FAME	Composition of mixture (%)			Time (h)	T (°C)	Reference
			C18:0	C18:1	C18:2			
9	**C1-Co**	ML	86	14	0	12	120	This Work
10	**C2-Ni**	ML	96	4	0	12	120	This Work
11	**C3-Pd**	ML	100	0	0	12	120	This Work
12	**C4-Co**	ML	100	0	0	12	120	This Work
13	**C5-Ni**	ML	100	0	0	12	120	This Work
14	**C6-Pd**	ML	3.21	28.47	68.29	6	120	This Work

2.2.4. Oxidative Stability by the Rancimat Method and Infrared Spectroscopy

The induction time or induction period is a term used to describe the time taken for a sample of biodiesel to react with oxygen and produce water-soluble volatile products that are detected in water by an increase in the conductivity of the water. The line of the curve is expected to show a steady conductivity until a time when the volatile products have diffused and dissolved in the water. A sample that takes a long period to show a change in conductivity shows that the sample is resistant to reacting with oxygen gas, and hence, the sample has high oxidative stability, whereas a sample that shows a quick change in the conductivity indicates a rapid onset of the oxidation reaction, showing that the sample has low oxidative stability. The oxidation reaction takes place when the C=C bonds in the sample react with oxygen to form different products. This section aims to establish the effect of the C18:2 and C18:1 composition of the biodiesel on its oxidation reaction that leads to the production of water-soluble oxidation products, which can be detected by a change in the conductivity of the water. The density and the viscosity of the samples were determined alongside the time it took for a change in the conductivity of the water (the induction period).

Here, the Rancimat method and IR were used to study the oxidative stability of biodiesel mixtures before and after hydrogenation. The Rancimat method is a well used approach to determine the amount of water-soluble volatile oxidation products that are produced from a sample, and it is approved by the BS EN 14112 European Standard 14112 [20,29]. In this method, 3 g of the sample was oxidized using constant airflow, while the diesel sample was heated at 110 °C in a round-bottom flask (Figure S16), and the volatiles produced were determined by measuring the changes in the conductivity of water in a flask filled with distilled water [13]. The induction period was determined from the intersection of the two lines of best fit of the conductivity vs. time plots. Figure 7 shows the changes in the density, induction period, and viscosity of the three samples (BD1, BD2, and BD3) before and after hydrogenation. Samples with high C18:2 chains

show low induction periods compared to the ones with fewer C18:2 chains. The induction period (IP) is observed to be high for BD1, which contains low amounts of C18:2 (12.5%), followed by BD3 (25.75%), and finally BD2 (29.5%). The high amount of C18:1 (41.54%) in BD1 compared to BD2 (45.3%) and BD3 (30.44%) does not seem to have a significant effect on the oxidation reaction, as the IP is highest in BD1 after hydrogenation.
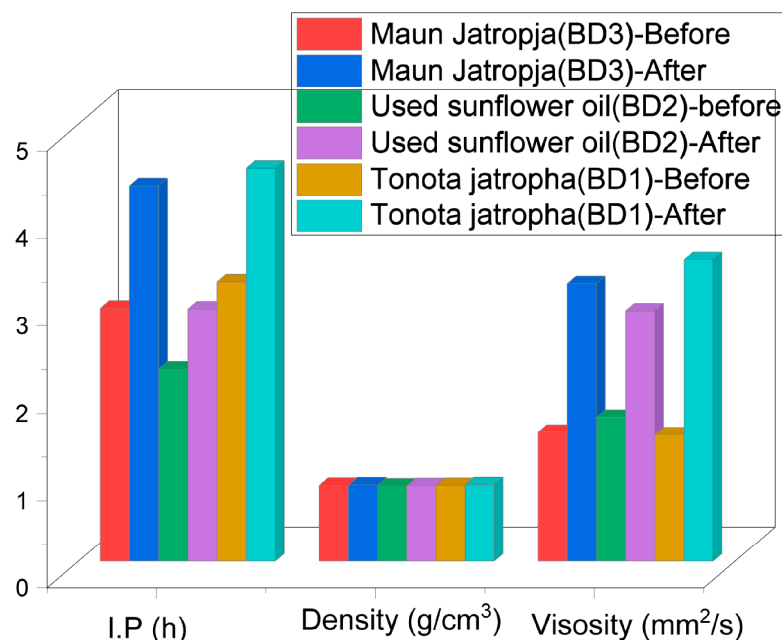

Figure 7. The comparison of the fuel properties of the biodiesels (BD1, BD2, and BD3).

Next, the properties of the hydrogenated biodiesel sample with the highest induction period were further compared to those of conventional LP5 diesel, as well as a blend of the biodiesel sample and conventional LP5 diesel. The LP5 was purchased from a local petrol station in Botswana. Blending biodiesel with commercial diesel is a well-proven and internationally adopted method of improving the oxidative stability, and in this work, the biodiesel sample was blended with 20% LP5 diesel before comparing the stability of this mixture with the hydrogenated biodiesel. Figure 8a shows that partially hydrogenating the samples improves the induction period from 3 to 5 h when compared with blended diesel, whereas blending the un-hydrogenated oil with 20% LP5 diesel improved the induction time from 3 to 7 h. While blending is the most often used method of controlling/improving the oxidative stability of the diesel, it is clear from this study that partial hydrogenation of the biodiesel is also effective at reducing the rate of auto-oxidation reactions, although the major problem of high viscosity (Figure 8b) might limit its applications. The low induction period in the hydrogenated sample (H-BD1) could be attributed to the build-up of C18:2 isomers that have been detected in the sample and are reported to negatively affect fuel properties.

The biodiesel samples BD1, H-BD1, BD1:LP5 blend, and BD1-BL (labeled BD1–20 in the staggered IR spectra) were analyzed using IR spectroscopy to determine the changes in the functional groups before and after 6 months of storage. These were compared to the IR of conventional LP5 diesel (Figure S17). The staggered IR spectra (Figure 9) show the CH stretches at 2853–305 cm^{-1}, and the C=O stretch is observed at 1730 cm^{-1} in all the analyzed samples, which confirms the expected functionalities of these samples [12]. The peak at 720 cm^{-1} shows the presence of the C18:2/C18:1 cis-isomer in all the biodiesel samples, while the C-C stretches are observed at 1300–1440 cm^{-1} [11,12,30]. The partially hydrogenated sample (H-BD1) shows no major changes in the functional groups as expected, and even after storage for 6 months, the functional groups show no changes, indicating negligible or no oxidative reactions to cause changes in the functional groups of the biodiesel.

However, the un-hydrogenated biodiesel sample after 6 months of storage (labeled BD1 stored 0.5 y in Figure 9) shows the significant onset of oxidation reactions leading to the appearance of a broad peak at 3490 cm^{-1}, which corresponds to the presence of the OH moiety and could be due to the formation of either aldehydes, ketones, lactones, caproic, or propionic acids [13]. In addition, the presence of the C-O-O stretch at 1125 cm^{-1} shows that the auto-oxidative reactions have degraded the fuel within 6 months of storage [12,31].
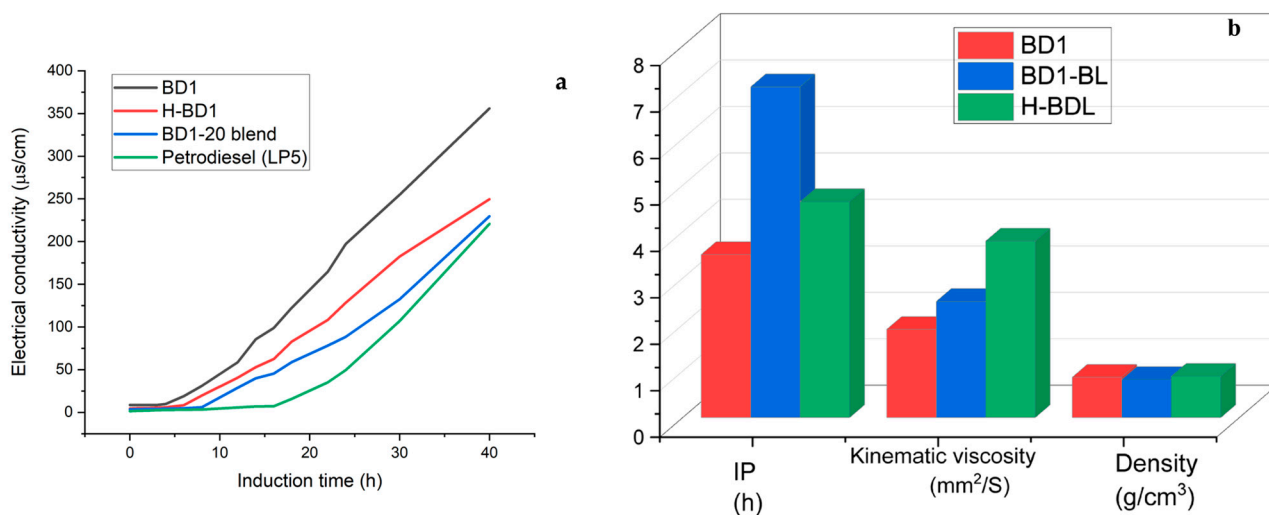

Figure 8. (**a**) Changes in the induction time of the biodiesel samples before and after hydrogenation in comparison with the effect of blending (BD1: jatropha biodiesel; H-BD1: partially hydrogenated jatropha biodiesel; BD1-BL: jatropha biodiesel blended with 20% LP5). (**b**) Comparative study of the density, kinematic viscosity, and induction period of the fuel samples: un-hydrogenated (BD1), partially hydrogenated BD1 (H-BD1), and jatropha biodiesel blended with 20% LP5 (BD1-BL).
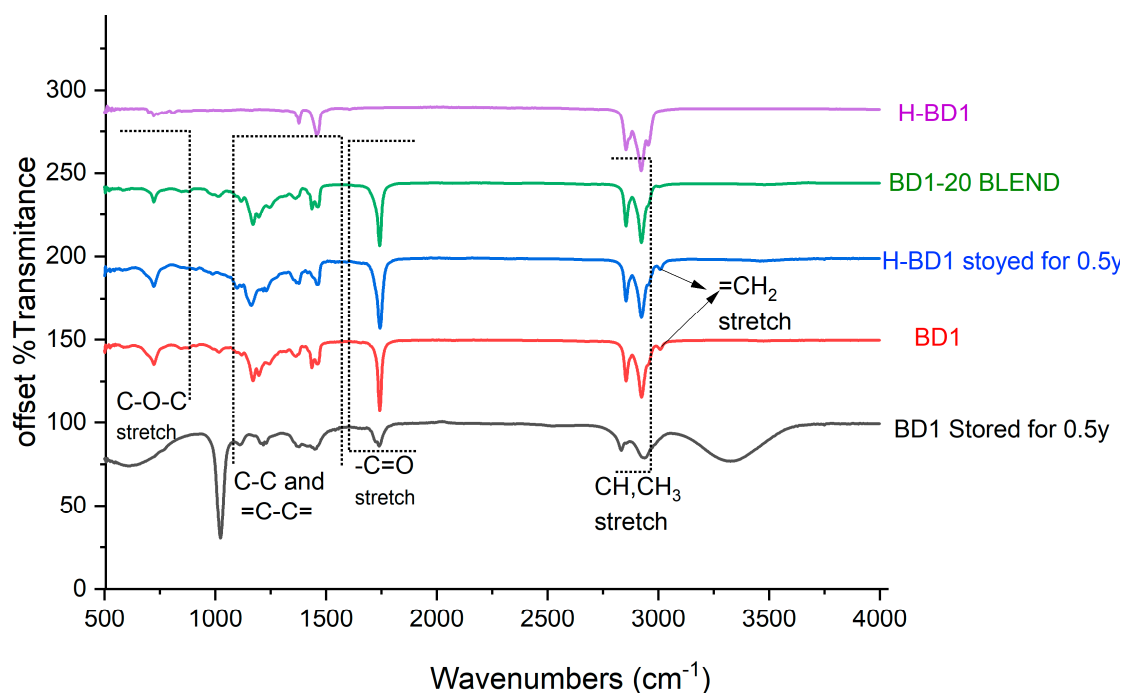

Figure 9. The FTIR analysis of the jatropha biodiesel (BD1), partially hydrogenated jatropha biodiesel (H-BD1), Un-hydrogenated jatropha biodiesel blended with 20% LP5 (BD1–20), and the diesel samples after 6 months of storage at room temperature.

3. Materials and Methods

All the seed oils were extracted from crushed seeds using hexane and methanol. Linoleic acid and other laboratory reagents/chemicals were purchased from Sigma Aldrich (Johannesburg, South Africa) and were used without further purification. All solvents were dried over molecular sieves 24 h before use. **L1**, **C1**, **C2**, and **C3** have been synthesized and characterized as reported in the literature [22].

3.1. Catalytic Hydrogenation Studies

Transfer hydrogenation studies were carried out in an autoclave stainless-steel batch reactor (50 mL), fitted in a heating block. The reaction mixture containing the catalyst, formic acid, triethyl amine, and the substrate was heated to the desired temperature after purging four times with nitrogen gas. The reaction was conducted at a stirring speed of 960 rpm for the required length of time. At the end of the reaction, the reactor vessel was cooled, and excess gas was released. The sample from the reactor was then dissolved in hexane, and the catalyst was removed by decanting. The filtrate was dried in an oven at 70 °C for an hour to remove the solvent (hexane). A sample of this mixture was then analyzed by ^{1}H NMR spectroscopy and gas chromatography to determine the components of the sample.

3.2. Synthesis of the Ligand and Metal Complexes

3.2.1. Synthesis of Ligand **L2**

To synthesize **L2**, 2 g of picolinic acid (16 mmol) was suspended in 100 mL of dry dichloromethane under an N_2 atmosphere. To this, 5 mL of thionyl chloride was added, and the reaction was allowed to continue at 40 °C. After 24 h, dichloromethane was removed under reduced pressure to obtain an orange oil. To this oil, 7 mL of triethylamine was added, and the mixture was placed in an ice bath. Next, 3.8 mL (16 mmol) of 3-aminopropyl triethoxysilane was slowly added. Then, 20 mL of dichloromethane was added, and the reaction mixture was stirred at room temperature for a further 24 h. The solvent was then removed under reduced pressure to obtain product **L2** as a brownish viscose oil that is soluble in chlorinated solvents and alcohols.

3.2.2. Synthesis of N-(3-(triethoxysilyl)propyl)picolinamido Cobalt(II) Chloride, **C4-Co**

A solution of ligand **L2** (0.311 g, 1.0 mmol) in dry dichloromethane (10 mL) was added to a solution of $CoCl_2$ (1.0 mmol) in dry methanol (20 mL) under nitrogen conditions. The reaction mixture was stirred for 24 h at room temperature. After completion of the reaction, the volume of solution was reduced to about 5 mL on a rotary evaporator, and the solid product was precipitated by adding ice-cold diethyl ether (15 mL). The product was filtered and washed with 3 parts diethyl ether (10 mL) and dried in vacuo. The $C_{15}H_{26}Cl_2CoN_2O_4Si$ had a molecular weight of 440.30, was obtained as a green solid, and was soluble in dichloromethane and methanol.

3.2.3. Synthesis of N-(3-(triethoxysilyl)propyl)picolinamido Nickel(II) Bromide, **C5-Ni**

A solution of ligand **L2** (0.311 g, 1.0 mmol) in dry methanol (10 mL) was added to the solution of $NiBr_2DME$ (1.0 mmol) in dry methanol (20 mL) under nitrogen conditions. The reaction mixture was stirred for 48 h at room temperature (27 °C). After completion of the reaction, the volume of solution was reduced to about 5 mL on a rotary evaporator, and the green solid product was precipitated by adding ice-cold hexane (20 mL). The solvent was decanted, and the resulting solid was washed with 3 parts diethyl ether (10 mL) and dried in vacuo. A green solid of molecular mass 528.97, which is soluble in methanol and dichloromethane, was obtained.

3.2.4. Synthesis of N-(3-(triethoxysilyl)propyl)picolinamido Palladium(II) Chloride, **C6-Pd**

A solution of ligand **L2** (0.311 g, 1.0 mmol) in dry dichloromethane (10 mL) was added to a solution of $Pd(NCME)_2Cl_2$ (1.0 mmol) in dry dichloromethane (20 mL) under nitrogen

conditions. The reaction mixture was stirred for 24 h. After completion of the reaction, the volume of solution was reduced to about 5 mL on a rotary evaporator, and the solid product was precipitated by adding ice-cold hexane (15 mL). The product was filtered, washed with 3 parts ice-cold hexane (10 mL), and dried in vacuo. The resulting dull-orange solid was found to be soluble in dichloromethane, chloroform, and methanol.

3.2.5. Determination of Composition of Mixture, Conversion, and Selectivity

To estimate the changes in the components of the diesel samples, the peak area was integrated using a computer-based software method. These peak areas are directly proportional to the amount of component that is reaching the detector (injected into the column), and the sample identities were confirmed from the corresponding m/z (mass to charge ratio) of the mass fragments. The equations below were used to determine the catalyst parameters shown.

$$\%\text{Conversion} = \left[\frac{S_{t0} - S_{tf}}{S_{t0}}\right] \times 100 \tag{1}$$

where S = substrate, t_0 is the start of the reaction, and t_f is the end of the reaction

$$\%\text{Selectivity of A} = \left[\frac{\text{Amount of A}}{\text{Total amount of products}}\right] \times 100 \tag{2}$$

4. Conclusions

In this work, new Ni, Co, and Pd complexes (**C4-Co**, **C5-Ni**, **C6-Pd**) have been synthesized, characterized, and used as catalysts for the hydrogenation of fatty acid methyl esters (FAMEs), alongside the known catalysts **C1-Co**, **C2-Ni**, and **C3-Pd**. The catalysts convert the C18:2 in both methyl linoleate and jatropha biodiesel in a 24 h reaction to C18:0 components, which is biodegradable wax. Reducing the reaction time is a significant factor in controlling the percentage of hydrogenated components under any tested reaction conditions. Reducing the reaction time from 12 h/24 h to 3 h leads to partially hydrogenated FAMEs, with 25.83% C16:0, 12.52% C18:2, 41.54% C18:1, 14.47% C18:0, and 3.0% isomers of C18:2 chains. The Rancimat method and infrared spectroscopy were used to evaluate the oxidative stability/the tendency of the oil samples to react with oxygen to produce water-soluble volatile products. Partial hydrogenation improves the induction time from 3 to 5 h, without a significant increase in viscosity, and it reduces the auto-oxidation radical reactions, giving a sample that can be stored for 6 months without deteriorating. Although partial hydrogenation of jatropha biodiesel improved the oxidative stability, build-up of the C18:2 isomers has been observed, which can affect the attractive fuel properties of the partially hydrogenated samples, even when detected at low amounts. In this study, a maximum of 3% isomers was detected at 3 h, while at 12 h, none were detected as a saturated/biodegradable product was obtained. However, the BD1-20 blend was shown to possess a better induction period (7 h) compared to the partially hydrogenated biodiesel. This study has demonstrated that partially hydrogenated biodiesel leads to improved oxidative stability of the biodiesel.

Supplementary Materials: The following supporting information can be downloaded at: https://www.mdpi.com/article/10.3390/catal14090653/s1, Figure S1: The ^{1}H NMR spectrum of ligand **L2** recorded in CDCl$_3$. Figure S2: The ^{13}C{^{1}H} NMR spectrum of ligand **L2** recorded in CDCl$_3$. Figure S3: FTIR of ligand **L2**. Figure S4: High-resolution ESI-MS of ligand **L2**. Figure S5: Structural determination of complex **C6-Pd** using ^{13}C NMR spectrometer recorded in CDCl$_3$. Figure S6a–c: IR spectra of complexes **C4-Co**, **C5-Ni**, and **C6-Pd**. Figure S7a–c: Electrospray ionization mass spectra for complexes **C4-Co**, **C5-Ni**, and **C6-Pd**. Figure S8: ^{1}H NMR spectrum showing the transesterification of linoleic acid using methanol to form methyl linoleate. Figure S9: The ^{1}H NMR spectrum of BD1. Figure S10: Visual of the changes in the flow of the biodiesel after hydrogenation. Figure S11: Mass spectrometer fragments of the components of BD1, in Figure 3. Figure S12: An example of a

chromatogram and the corresponding mass fragments for all the detected peaks for entry 2 Table 3. No C18:1 detected. Figure S13: Corresponding mass fragments for the detected peaks for Figure 5, Where C16:0 = m/z 270, C18:2 = m/z 294, C18:1 = m/z 296, and C18:0 = m/z 298. Figure S14: Identification of compounds in biodiesel sample BD3 after hydrogenation and the corresponding mass fragments. Figure S15: Identification of compounds in biodiesel sample BD2 after hydrogenation and the corresponding mass fragments. Figure S16: Experimental setup for the conductivity measurements. Figure S17: FTIR spectrum of commercial diesel. Table S1: Different oil components of jatropha and methyl linoleate. References [32–34] are cited in the Supplementary Materials.

Author Contributions: Conceptualization, N.H.d.L., O.A.O. and J.D.; methodology, F.P.S.; software, F.P.S.; validation, N.H.d.L., J.D. and O.A.O.; formal analysis, F.P.S.; investigation, F.P.S.; catalytic reactor resources, B.C.E.M.; data curation, F.P.S.; writing—original draft preparation, F.P.S.; writing—review and editing, N.H.d.L., O.A.O. and J.D.; visualization, N.H.d.L., J.D. and F.P.S.; supervision, O.A.O., J.D. and N.H.d.L.; project administration, N.H.d.L.; funding acquisition, N.H.d.L. All authors have read and agreed to the published version of the manuscript.

Data Availability Statement: The data supporting this investigation are available as electronic supporting information (ESI).

Conflicts of Interest: The authors declare no conflicts of interest.

References

1. Paparao, J.; Murugan, S. Dual-Fuel Diesel Engine Run with Injected Pilot Biodiesel-Diesel Fuel Blend with Inducted Oxy-Hydrogen (HHO) Gas. *Int. J. Hydrogen Energy* **2022**, *47*, 17788–17807. [CrossRef]
2. Hossain, M.; Israt, S.S.; Muntaha, N.; Jamal, M.S. Effect of Antioxidants and Blending with Diesel on Partially Hydrogenated Fish Oil Biodiesel to Upgrade the Oxidative Stability. *Bioresour. Technol. Rep.* **2022**, *17*, 100938. [CrossRef]
3. Moser, B.R. Biodiesel Production, Properties, and Feedstocks. In *Biofuels: Global Impact on Renewable Energy, Production Agriculture, and Technological Advancements*; Springer: Heidelberg, Germany, 2011; ISBN 9781441971449.
4. Muralidhara, D.M.; Banapurmath, N.R.; Udayaravi, M.; Prabhakar Reddy, C.; Harari, P.A.; Karthik, T. Effect of Hydrogen Flow Rates on the Performance of Two Biodiesels Fuelled Dual Fuel Engine. *Mater. Today Proc.* **2022**, *49*, 2189–2196. [CrossRef]
5. Brandt, P.; Hedberg, C.; Andersson, P.G. New Mechanistic Insights into the Iridium ± Phosphanooxazoline-Catalyzed. *Chem.-A Eur. J.* **2003**, *9*, 339–347. [CrossRef] [PubMed]
6. Hanis, S.; Sayid, Y.; Hanis, N.; Hanapi, M.; Azid, A. A Review of Biomass-Derived Heterogeneous Catalyst for a Sustainable Biodiesel Production. *Renew. Sustain. Energy Rev.* **2017**, *70*, 1040–1051. [CrossRef]
7. Adu-Mensah, D.; Mei, D.; Zuo, L.; Zhang, Q.; Wang, J. A Review on Partial Hydrogenation of Biodiesel and Its Influence on Fuel Properties. *Fuel* **2019**, *251*, 660–668. [CrossRef]
8. Atabani, A.E.; Silitonga, A.S.; Badruddin, I.A.; Mahlia, T.M.I.; Masjuki, H.H.; Mekhilef, S. A Comprehensive Review on Biodiesel as an Alternative Energy Resource and Its Characteristics. *Renew. Sustain. Energy Rev.* **2012**, *16*, 2070–2093. [CrossRef]
9. Chen, S.-Y.; Attanatho, L.; Mochizuki, T.; Abe, Y.; Toba, M.; Yoshimura, Y.; Kumpidet, C.; Somwonhsa, P.; Lao-ubol, S. Upgrading of Palm Biodiesel Fuel over Supported Palladium Catalysts. *Comptes Rendus Chim.* **2016**, *19*, 1166–1173. [CrossRef]
10. Olaoye, O.E.; Oyetunji, O.; Makhubela, B.C.E.; Kumar, G.; Darkwa, J. Hydrogenation of Biodiesel Catalysed by Pyrazolyl Nickel(Ii) and Palladium(Ii) Complexes. *RSC Sustain.* **2023**, *1*, 1814–1825. [CrossRef]
11. Flitsch, S.; Neu, P.M.; Schober, S.; Kienzl, N.; Ullmann, J.; Mittelbach, M. Quantitation of Aging Products Formed in Biodiesel during the Rancimat Accelerated Oxidation Test. *Energy Fuels* **2014**, *28*, 5849–5856. [CrossRef]
12. Zhou, J.; Xiong, Y.; Shi, Y. Antioxidant Consumption Kinetics and Shelf-Life Prediction for Biodiesel Stabilized with Antioxidants Using the Rancimat Method. *Energy Fuels* **2016**, *30*, 10534–10542. [CrossRef]
13. Aparicio, R.; Roda, L.; Albi, M.A.; Gutiérrez, F. Effect of Various Compounds on Virgin Olive Oil Stability Measured by Rancimat. *J. Agric. Food Chem.* **1999**, *47*, 4150–4155. [CrossRef] [PubMed]
14. Wongjaikham, W.; Kongprawes, G.; Wongsawaeng, D.; Ngaosuwan, K.; Kiatkittipong, W.; Hosemann, P.; Assabumrungrat, S. Highly Effective Microwave Plasma Application for Catalyst-Free and Low Temperature Hydrogenation of Biodiesel. *Fuel* **2021**, *305*, 121524. [CrossRef]
15. Thunyaratchatanon, C.; Jitjamnong, J.; Luengnaruemitchai, A.; Numwong, N.; Chollacoop, N.; Yoshimura, Y. Influence of Mg Modifier on Cis-Trans Selectivity in partial hydrogenation of biodiesel using different metal types. *Appl. Catal. A Gen.* **2016**, *520*, 170–177. [CrossRef]

16. Kongprawes, G.; Wongsawaeng, D.; Hosemann, P.; Ngaosuwan, K.; Kiatkittipong, W.; Assabumrungrat, S. Dielectric Barrier Discharge Plasma for Catalytic-Free Palm Oil Hydrogenation Using Glycerol as Hydrogen Donor for Further Production of Hydrogenated Fatty Acid Methyl Ester (H-FAME). *J. Clean. Prod.* **2023**, *401*, 136724. [CrossRef]
17. Peer, M.S.; Kasimani, R.; Rajamohan, S.; Ramakrishnan, P. Experimental Evaluation on Oxidation Stability of Biodiesel/Diesel Blends with Alcohol Addition by Rancimat Instrument and FTIR Spectroscopy. *J. Mech. Sci. Technol.* **2017**, *31*, 455–463. [CrossRef]
18. Figueredo, I.D.M.; Rios, M.A.D.S.; Cavalcante, C.L., Jr.; Luna, F.M.T. Effects of Amine and Phenolic Based Antioxidants on the Stability of Babassu Biodiesel Using Rancimat and Differential Scanning Calorimetry Techniques. *Ind. Eng. Chem. Res.* **2020**, *59*, 18–24. [CrossRef]
19. de la Presa-Owens, S.; Lopez-Sabater, M.C.; Rivero-Urgell, M. Shelf-Life Prediction of an Infant Formula Using an Accelerated Stability Test (Rancimat). *J. Agric. Food Chem.* **1995**, *43*, 2879–2882. [CrossRef]
20. De Menezes, L.C.; De Sousa, E.R.; Da Silva, G.S.; Marques, A.L.B.; Viegas, H.D.C.; Dos Santos, M.J.C. Investigations on Storage and Oxidative Stability of Biodiesel from Different Feedstocks Using the Rancimat Method, Infrared Spectroscopy, and Chemometry. *ACS Omega* **2022**, *7*, 30746–30755. [CrossRef]
21. Kirubakaran, M.; Selvan, V.A.M. A Comprehensive Review of Low Cost Biodiesel Production from Waste Chicken Fat. *Renew. Sustain. Energy Rev.* **2018**, *82*, 390–401. [CrossRef]
22. Sejie, F.P.; Oyetunji, O.A.; Darkwa, J.; Beas, I.N.; Makhubela, B.C.E.; Dzade, N.Y.; de Leeuw, N.H. The Transfer Hydrogenation of Cinnamaldehyde Using Homogeneous Cobalt(II) and Nickel(II) (E)-1-(Pyridin-2-Yl)-N-(3-(Triethoxysilyl)Propyl)Methanimine and the Complexes Anchored on Fe_3O_4 Support as Pre-Catalysts: An Experimental and In Silico Approach. *Molecules* **2023**, *28*, 659. [CrossRef] [PubMed]
23. Sejie, F.P. The Synthesis and Characterization of the Homogeneous and Their Fe_3O_4 Picolinyl Metal Complexes for Application as Hydrogenation Catalysts. Ph.D. Thesis, University of Botswana, Gaborone, Botswana, May 2023.
24. Behr, A.; Vorholt, A.J. *Homogeneous Catalysis with Renewables*; Springer: New York, NY, USA, 2017; Volume 39, ISBN 978-3-319-54159-4.
25. Liu, W.; Xu, L.; Lu, G.; Zhang, H. Selective Partial Hydrogenation of Methyl Linoleate Using Highly Active Palladium Nanoparticles in Polyethylene Glycol. *ACS Sustain. Chem. Eng.* **2017**, *5*, 1368–1375. [CrossRef]
26. Frankel, E.N.; Emken, E.A.; Peters, H.M.; Davison, V.L.; Butterfield, R.O. Homogeneous Hydrogenation of Methyl Linoleate Catalyzed by Iron Pentacarbonyl. Characterization of Methyl Octadecadienoate—Iron Tricarbonyl Complexes1. *J. Org. Chem.* **1964**, *29*, 3292–3297. [CrossRef]
27. Abley, P.; McQuillin, F.J. Homogeneous Hydrogenation of Methyl Linoleate by Means of Nickel and Rhodium Complexes in Dimethylformamide. *J. Catal.* **1972**, *24*, 536–540. [CrossRef]
28. Bailar, J.C. The Selective Homogeneous Hydrogenation of Soybean Methyl Esters. *J. Am. Oil Chem. Soc.* **1970**, *47*, 475–477. [CrossRef]
29. *BS EN 14112*; Fat and Oil Derivatives. Fatty Acid Methyl Esters (FAME). Determination of Oxidation Stability (Accelerated Oxidation Test). European standards: Plzen, Czech Republic, 2020.
30. Quaranta, E.; Dibenedetto, A.; Colucci, A.; Cornacchia, D. Partial Hydrogenation of FAMEs with High Content of C18:2 Dienes. Selective Hydrogenation of Tobacco Seed Oil-Derived Biodiesel. *Fuel* **2022**, *326*, 125030. [CrossRef]
31. Kongprawes, G.; Wongsawaeng, D.; Hosemann, P.; Ngaosuwan, K.; Kiatkittipong, W.; Assabumrungrat, S. Improvement of Oxidation Stability of Fatty Acid Methyl Esters Derived from Soybean Oil via Partial Hydrogenation Using Dielectric Barrier Discharge Plasma. *Int. J. Energy Res.* **2021**, *45*, 4519–4533. [CrossRef]
32. Atkinson, B.N.; Chhatwal, A.R.; Williams, J.M.J. Catalytic amide bond forming methods. In *Applied Homogeneous Catalysis with Organometallic Compounds: A Comprehensive Handbook in Three Volumes*; Wiley: Hoboken, NJ, USA, 2012. [CrossRef]
33. Henderson, W.; McIndoe, J.S. *Mass Spectrometry of Inorganic and Organometallic Compounds: Tools—Techniques—Tips*; Wiley: Hoboken, NJ, USA, 2005; Volume 9. [CrossRef]
34. Park, J.K.; Shin, W.K.; An, D.K. New and efficient synthesis of amides from acid chlorides using diisobutyl(amino)aluminum. *Bull. Korean Chem. Soc.* **2013**, *34*, 1592–1594. [CrossRef]